ОБЪЕДИНЕННЫЙ ИНСТИТУТ ЯДЕРНЫХ ИССЛЕДОВАНИЙ

Лаборатория теоретической физики им. Н. Н. Боголюбова

На правах рукописи

Нгуен Дань Тунг

Флуктуации заряда и сверхпроводимость в сильно коррелированных электронных системах

Специальность: 1.3.3 – Теоретическая физика

АВТОРЕФЕРАТ

диссертации на соискание ученой степени
кандидата физико-математических наук

Дубна – 2022

JOINT INSTITUTE FOR NUCLEAR RESEARCH

N. N. Bogoliubov Laboratory of Theoretical Physics

Nguyen Danh Tung

Charge fluctuations and superconductivity in strongly correlated electronic systems

Specialty: 1.3.3 — Theoretical physics

ABSTRACT

of the dissertation to obtain the academic degree of
Doctor of Philosophy in Physics and Mathematics

Dubna – 2022

The dissertation was performed at N. N. Bogoliubov Laboratory of Theoretical Physics (BLTP) of the Joint Institute for Nuclear Research.

Scientific Supervisor

Yushankhai Victor Yulievich
Doctor of Physical and Mathematical Sciences
Leading Researcher, Bogolyubov Laboratory of Theoretical Physics (BLTP), JINR

The electronic version of the dissertation is available at the official web-site of JINR: https://dissertations.jinr.ru. The printed version of the dissertation is available at the JINR Science and Technology Library (Dubna, Moscow Region, Joliot-Curie Str., 6) - http://lib.jinr.ru/english.html.

Scientific secretary of the dissertation council,
PhD in Physics Bystritsky Yury Mikhailovich

General description of the work

Relevance of the topic

Transition metal oxides (TMOs) form probably one of the most interesting classes of solids, exhibiting a wide variety of structures and properties. The unique electrical and magnetic properties of TMOs have attracted the interest of theoretical physicists and technology developers for their applicability. Recently, experiments have provided observable evidence of many exotic phenomena occurring in TMOs, such as charge density waves (CDW) (e.g. $K_{0.3}MoO_3$), charge ordering (e.g. Fe_3O_4), and defect ordering (e.g. $Ca_2Mn_2O_5$, $Ca_2Fe_2O_5$). TMOs can range from ferromagnetic (e.g. CrO_2, $La_{0.5}Sr_{0.5}MnO_3$) to antiferromagnetic (AFM) (e.g. NiO, $LaCrO_3$). Many oxide compounds have switchable orientation states such as ferroelectric (e.g. $BaTiO_3$, $KNbO_3$) and ferroelastic [e.g. $Gd_2(MoO_4)_3$]. Some TMOs have metallic properties (e.g. RuO_2, ReO_3, $LaNiO_3$), while others have highly insulating properties (e.g. $BaTiO_3$). Several oxides exhibit co-existence of metallic and non-metallic properties (e.g. $Lu_2Rh_2O_7$). Among them, the phenomenon of high-temperature superconductivity (HTSC) in cuprates is one of the issues of interest to solid-state physicists.

The unusual properties of TMOs are clearly due to the unique nature of the outer d or f electrons. The d electrons are localized, their wavefunctions are restricted in a small space around the atom. They are distributed inside a sphere with small radius, this makes the chance of electrons meeting each other higher than other bands, the on-site Coulomb interaction (CI) is thus larger. Therefore, many TMOs belong to strongly correlated materials which have incompletely filled d- or f-electron shells with narrow energy bands. In these materials, transition metal can easily combine with oxygen to form covalent bond. It gives all s electrons and some d electrons to oxygen, there are only d or f electrons remaining in its outer shell. If TMOs contain the alkaline or rare earth elements, they can provide additional electrons to oxygen. Depending on atomic radius, they can distort the lattice structure. Therefore, the basic electronic structures of TMOs origin from transition metal d bands as frontier bands, oxygen p bands the second most energetic bands staying at the Fermi level, other bands have less significant impact to the electronic properties of these materials.

The theoretical understanding of the properties of various TMO materials is one of major challenges to the modern condensed matter theory. The behavior of electrons and spinons in these materials cannot be effectively described by traditional one-electron theories, it requires more modern methods to treat these strongly correlated systems which are the reason for the very rich physical properties in TMOs and represented by complicated phase diagrams. Many theories have been proposed to describe corelation electrons in TMOs, among them the dynamical mean field theory (DMFT) is a numerical method that has proved to be very effective. In addition, the Hubbard model is a simple, but very useful model for the general description of corelated materials. In the limit of strong correlations, the Hubbard model can be reduced to the $t-J$ model with the intersite Coulomb repulsion V, the so called $t-J-V$ model, which turns out to

be an effective model for cuprate HTSC. Therefore understanding of physical properties of highly correlated systems and study microscopic models of strong correlations are the actual tasks.

Purpose and objectives of the thesis

The goal of the dissertation is the theoretical study of several properties of TMOs based on models of strongly correlated electron systems: the metal-insulator transition (MIT) in the ionic Hubbard model (IHM), static and dynamic charge fluctuations (CFs) and HSTC within the microscopic $t-J-V$ model.

To achieve these goals, the following tasks have been formulated and studied:

1. Obtaining the phase diagram of the half-filled IHM with the on-site Coulomb repulsion U and the ionic energy Δ by mean of the coherent potential approximation (CPA). When the system is in the metallic phase a dependence of the dc conductivity on the model parameters is calculated.

2. Calculation of the static charge susceptibility (SCS) and the dynamic charge susceptibility (DCS) in strongly correlated electronic systems within the two-dimensional $t-J-V$ model. The spectral density and the spectrum of charge excitations as functions of doping and other model parameters are obtained with the use of the equation of motion method for the relaxation functions in terms of the Hubbard operators (HOs).

3. Application of the extended $t-J-V$ model where the intersite Coulomb repulsion and the electron-phonon interaction (EPI) are taken into account to investigate electronic spectrum and superconductivity in cuprate HTSC. The Dyson equation for the normal and anomalous (pair) Green functions (GFs) is used in the special form where the self-energy is taken in the self-consistent Born approximation (SCBA). Superconducting T_c dependence on EPI and spin-fluctuation interaction is studied.

Scientific novelty

Phase diagram in IHM was studied by using CPA. The equaions of local GFs of sub-lattices were derrived, the solutions were then found by developing numerical calculations. The obtained results partially contribute to the debates about the phase diagrams of related materials. They are in good agreement with the results of previous publications.

CDWs have been studied in the $t-J-V$ model, where compared to the original $t-J$ model, the intersite CI between electrons has been introduced. Using the memory function method, SCS and DCS were calculated. Numerical methods are developed to show the dependence of the above quantities on the parameters of the model.

Electronic spectrum and superconductivity have been studied in frame work of the extended $t-J-V$ model. Using the projection method we obtain the Dyson equation for the GF. The normal and superconducting states are considered. A numerical program is used to show the dependence of the spectral function and the self-energy on the model parameters. The obtained

results are in good agreement with the previous theoretical and experimental results and can be used as a reference for further studies on superconductivity.

The main results of the thesis submitted for defense:

1. The phase diagram was investigated using CPA in the half-filled ionic Hubbard model (IHM). The metallic phase was proved to be sandwiched between the band insulator (BI) phase and the Mott insulator (MI) one. The maximum value of the temperature dependent conductivity $\sigma_{max}(T)$ as a function of on-site Coulomb repulsion U occurs near to $U \approx 2\Delta$ and $\sigma_{max}(T)$ decreases with increasing T.

2. The behavior of static and dynamic charge susceptibility have been considered in the framework of the $t-J-V$ model with the Green function (GF) technique. It is shown that with increasing the intersite Coulomb repulsion V, the static charge susceptibility $\chi(q)$ grows without limit (i.e. $1/\chi(q)$ vanishes), and charge density waves arise in the system either along the diagonal of the unit cell or along the edge of the unit cell.

3. Within the $t-J-V$ model, the damping of dynamic charge fluctuations derived from the calculated imaginary part of the memory function and the GF technique was analyzed for a large range of doping δ, $0 < \delta \leq 0.3$. The behavior was obtained to change from a broad spectrum of overdamped charge fluctuations at $\delta \approx 0.1$ to the Fermi-like behavior for $\delta > 0.1$.

4. The extended $t-J-V$ model with the electron-phonon interaction was applied to study electronic spectrum and superconductivity for strongly correlated electron system. The Dyson equation for the normal and anomalous GFs was derived in term of Hubbard operators and the self-energy was obtained in the self-consistent Born approximation.

5. Within the approach defined in the point 4 and applied for normal electronic properties, the calculated GFs revealed a transition from well defined quasiparticle electron excitations to overdamped broad excitations. The sharp Fermi surface in the mean-field approximation in the form of hole pockets at low doping is accompanied by the transformation to arc Fermi surface.

6. The statement on the dominance of the kinematic interaction in the spin fluctuation mechanism of superconducting pairing, earlier obtained in $t-J$ model, was reexamined in the framework of the extended $t-J-V$ model including electron-phonon coupling $\sim g$. The statement was confirmed in a wide range of physically significant parameters V and g.

Approbation of the thesis

The results of the dissertation were presented **personally** by the author at the seminars of the Laboratory of Theoretical Physics (BLTP), JINR as well as at conferences:

1. The XXII International Scientific Conference of Young Scientists and Specialists (AYSS-2018), 23-27 April 2018), JINR, Dubna, Russia.

2. Meeting of the Programme Advisory Committee for Condensed Matter Physics, 14–15 June 2018, Dubna, Rusia.

3. XXII Scientific School of Young Scientists and Specialists of JINR (LIPNYA 2018), 20-22 July 2018, Dubna, Russia.

4. XXII Training Course in the Physics of Strongly Correlated Systems, 1-12 October, 2018, Vietri sul Mare (Salerno), Italy.

5. The XXIII International Scientific Conference of Young Scientists and Specialists (AYSS-2019), 15-19 April 2019, JINR, Dubna, Russia.

6. Autumn School on Correlated Electrons: Topology, Entanglement, and Strong Correlations, 21-25 September 2020, Forschungszentrum Jülich — Online-Edition.

7. The XXIV International Scientific Conference of Young Scientists and Specialists (AYSS-2020), 9-13 November 2020, Dunba, Russia.

List of publications

The results of the study are published in the following four articles in peer-reviewed journals included in the list:

1. Nguen Dan Tung, Hoang Anh Tuan, Conductivity in the half-filled ionic Hubbard model Communications in Physics, Vol. **24**, No. 3S2, pp. 34-38. (2014).

2. Dan Tung Nguen, N. M. Plakida, Static charge susceptibility in the t-J-V model, Theoretical and Mathematical Physics, **194**, 127-141 (2018).

3. Nguen Dan Tung, N. M. Plakida, Charge dynamics in strongly-correlated electronic systems, International Journal of Modern Physics B,**32**, No. 29 1850327 (22 pages), (2018).

4. Nguen Dan Tung, A. Vladimirov, N. M. Plakida, Electronic spectrum and superconductivity in the extended t-J-V model, Physica C:**587**, 1353900 (1-16), (2021).

Personal contribution of the author

The content of the dissertation and the provisions submitted for defense, reflect the personal contribution of the author. The author took an active part in all stages of the work. His contribution was decisive in carrying out the analytical and numerical calculations, the development of algorithms, as well as the preparation and writing of articles with the supervisor. All results submitted for defense were obtained personally by the author.

Confidence level

The reliability of the results obtained is based on the use of widely recognized and proven theoretical methods, such as CPA, memory function, projection method, etc., which have been used to study strongly correlated systems previously. The similarity of the obtained results with the results of previous studies is a good reason for their reliability.

The structure and amount of the thesis

The dissertation consists of introduction, 3 chapters, conclusion, bibliography and 7 appendices. The general volume of the dissertation is 84 pages, including 53 figuress and 1 table. The bibliography includes 198 titles on 10 pages.

Content of the work

In **Introduction** we demonstrate the relevance of the disertation, determine the main purpose and objectives of the research, argue about the novelty and practical significance of the work, and the reliability. Results are approved at conferences, scientific seminars, lists of publications. The brief description of the disertation structure is given.

In the **First Chapter** we discuss on MIT in the IHM on a bipartite lattice (sub-lattices A and B) which has the Hamiltonian:

$$H = -t \sum_{i\in A, j\in B, \sigma} [c^+_{i\sigma} c_{j\sigma} + c^+_{j\sigma} c_{i\sigma}] + U \sum_i n_{i\sigma} n_{i\overline{\sigma}} + \varepsilon_A \sum_{i\in A} n_i + \varepsilon_B \sum_{j\in B} n_j - \mu \sum_i n_i, \tag{1}$$

where $c_{i\sigma}(c^+_{i\sigma})$ annihilates (creates) an electron with spin σ at site i, $n_{i\sigma} = c^+_{i\sigma} c_{i\sigma}$ and $n_i = \sum_\sigma n_{i\sigma}$ is the electron number operator at site i. U is the on-site Coulomb repulsion, t is the nearest neighbor hopping parameter, $\varepsilon_A = \Delta$ and $\varepsilon_B = -\Delta$ are the ionic energies. The chemical potential $\mu_A = \mu_B = \mu$ is chosen so that the average occupancy equal 1 (half-filling), as a result $\mu = U/2$.

Using alloy approach, we can rewrite the Hamiltonian (1) as the one-particle Hamiltonian with disorder:

$$H = -t \sum_{<ij>\sigma} [a^+_{i\sigma} b_{j\sigma} + b^+_{j\sigma} a_{i\sigma}] + \sum_{i\in A,\sigma} E_{A,\sigma} a^+_{i\sigma} a_{i\sigma} + \sum_{j\in B,\sigma} E_{B,\sigma} b^+_{j\sigma} b_{j\sigma}, \tag{2}$$

where

$$E_{\alpha,\sigma} = \begin{cases} \varepsilon_\alpha - U/2, & \text{with probability } 1 - n_{\alpha,\overline{\sigma}} \\ \varepsilon_\alpha + U/2, & \text{with probability } n_{\alpha,\sigma}, \end{cases} \tag{3}$$

here $\alpha = A, B$, and $n_{\alpha,\sigma}$ is the average occupation of electrons with spin σ in α sub-lattice. Introduce retarded anticommutator GFs $G^{il}_{A\sigma}(t-t') = \langle\langle a_{i\sigma}(t); a^\dagger_{j\sigma}(t')\rangle\rangle$ and $G^{ji}_{BA\sigma}(t-t') = \langle\langle b_{j\sigma}(t); a^\dagger_{i\sigma}(t')\rangle\rangle$, writing down equations of motion for the GFs, using semi-density of state (DOS) function $\rho_0(\varepsilon) = 2/(\pi W^2)\sqrt{W-\varepsilon^2}$, we obtain

$$G_{A\sigma}(\omega) = \frac{2}{W^2} b \left(1 - \sqrt{1 - \frac{W^2}{ab}}\right), \tag{4}$$

and similar for $G_{B\sigma}(\omega)$ where $a = \omega - \Sigma_{A\sigma}(\omega)$ and $b = \omega - \Sigma_{B\sigma}(\omega)$, $\Sigma_\alpha(\omega)$ is the self-energy of the α sub-lattice, W is half-width of the band to be set as the energy unit. The CPA demands that the scattering matrix at site l, $T_l(\omega) = \frac{V_l(\omega)}{1 - V_l(\omega) G(\omega)}$ vanishes on average, where $V_l(\omega) = E_{\alpha\sigma} - \Sigma_{\alpha\sigma}(\omega)$ is perturbation potential at site l. This yields

$$\begin{aligned} &\frac{1}{16} G^2_{\overline{\alpha}}(\omega) G_\alpha(\omega) + \frac{1}{2}(\varepsilon_\alpha - \omega) G_{\overline{\alpha}}(\omega) G_\alpha(\omega) + \big[(\varepsilon_\alpha - \omega)^2 - \frac{U^2}{4}\big] G_\alpha(\omega) \\ &+ \frac{1}{4} G_{\overline{\alpha}}(\omega) + \varepsilon_\alpha - \omega - \frac{U}{2}(n_\alpha - 1) = 0. \end{aligned} \tag{5}$$

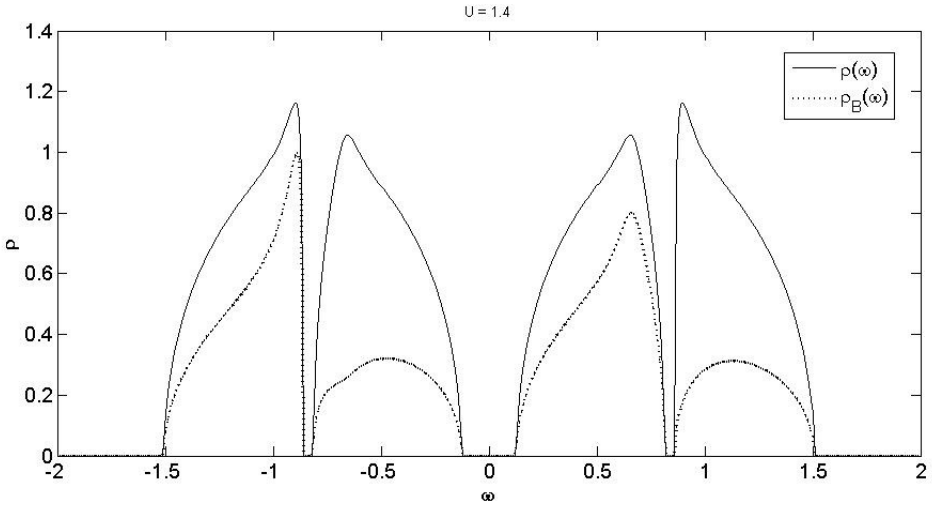

Fig. 1: DOS $\rho(\omega)$ and $\rho_B(\omega)$ with $\Delta = 0.1$, $U = 1.4$.

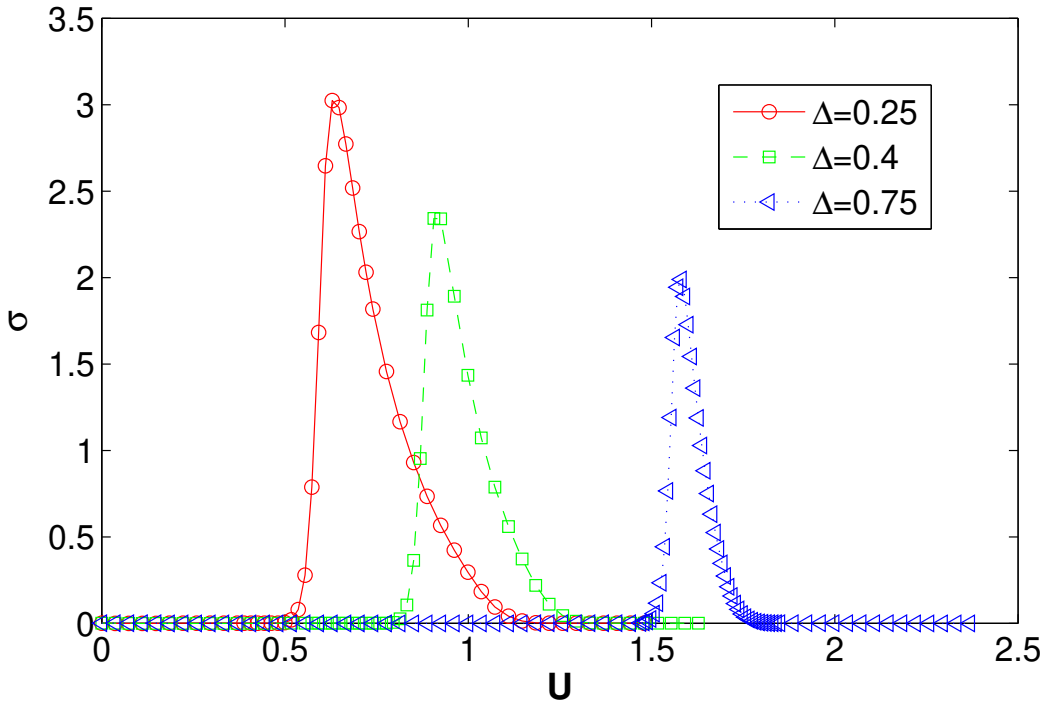

Fig. 2: Conductivity as a function of U for $T = 0$ and different values of Δ.

Equation (5) must be solved with $n_A + n_B = 2$, where $n_\alpha = -2/\pi \int_\infty^0 ImG_\alpha(\omega)d\omega$. The solution can be used to determine the local one-particle DOS $\rho_\alpha(\omega) = (-1/\pi)ImG_\alpha(\omega)$, the staggered charge density $n_B - n_A$ and the charge gap as functions of the model parameters U, Δ and temperature T.

Figure 1 shows DOS $\rho_B(\omega)$ and the average DOS $\rho(\omega) = \frac{1}{2}[\rho_A(\omega) + \rho_B(\omega)]$ as functions of energy with $\Delta = 0.1$ and $U = 1.4$. For fixed Δ there is a gap between the two bands for small U, the material is considered to be in the BI state. As U increases, it affects the displacement of the energy bands, at $U = 0.85$ there is overlap of two energy bands into a single region, the material becomes metal ($\rho(0) > 0$). Keep increasing U the material becomes MI, two more energy bands appear and there is a gap between the regions.

The conductivity corresponding to the metallic phase with three values of Δ is plotted in Fig. 2. It is interesting to note that for intermediate and large Δ the largest conductivity occurs near the special value $U = 2\Delta$ as one might expect from the atomic limit case. Similar behavior of the conductivity in the half-filled IHM was also found in determinant quantum Monte Carlo (DQMC) studies [1,2]. In addition, the largest conductivity $\sigma_{max}(\Delta)$ decreases with increasing Δ. The main results of this chapter are published in Ref.1 from the List of publications above.

In the **Second Chapter** we consider the $t-J-V$ model where in addition to the conventional hopping t and exchange interaction J terms the intersite Coulomb repulsion V is taken into account. It is convenient to use the HO technique [3, 4] and to write the model as follow (see., e.g., [5]):

$$\begin{aligned} H &= H_t + H_J + H_c = -\sum_{i\neq j,\sigma} t_{ij} X_i^{\sigma 0} X_j^{0\sigma} - \mu \sum_{i\sigma} X_i^{\sigma\sigma} \\ &+ \frac{1}{4}\sum_{i\neq j,\sigma} J_{ij}\left(X_i^{\sigma\bar{\sigma}} X_j^{\bar{\sigma}\sigma} - X_i^{\sigma\sigma} X_j^{\bar{\sigma}\bar{\sigma}}\right) + \frac{1}{2}\sum_{i\neq j} V_{i,j} N_i N_j, \end{aligned} \tag{6}$$

where the HOs $X_i^{\alpha\beta} = |i\alpha\rangle\langle i\beta|$ describe the transitions from the state $|i,\beta\rangle$ to the state $|i,\alpha\rangle$ on the lattice site i for the three electronic states with spin $\sigma/2$, $\sigma = \pm 1$ ($\bar{\sigma} = -\sigma$) : the unoccupied state ($\alpha, \beta = 0$) and two singly occupied states ($\alpha, \beta = \sigma$). Here $t_{ij} = t\delta_{j,i+\mathbf{a}_1} + t'\delta_{j,i+\mathbf{a}_2} + t''\delta_{j,i+\mathbf{a}_3}$ where t, t', t'' are the hopping parameters between the first $\mathbf{a}_1 = \pm a_x, \pm a_y$, second $\mathbf{a}_2 = \pm(a_x \pm a_y)$, and third $\mathbf{a}_3 = \pm 2a_x, \pm 2a_y$ neighbors, respectively ($a_x = a_y$ - are the two-dimensional lattice constants). $J_{ij} = J\delta_{j,i+\mathbf{a}_1}$ is the exchange interaction for the nearest neighbors. The intersite CI $V_{ij} = V_1\delta_{j,i+\mathbf{a}_1} + V_2\delta_{j,i+\mathbf{a}_2}$ where V_1 and the V_2 are CI between the first and the second neighbors, respectively. The number and spin operators in HO representation read

$$N_i = \sum_\sigma X_i^{\sigma\sigma}, \tag{7}$$

$$S_i^\sigma = X_i^{\sigma\bar{\sigma}}, \quad S_i^z = (\sigma/2)\left(X_i^{\sigma\sigma} - X_i^{\bar{\sigma}\bar{\sigma}}\right). \tag{8}$$

The chemical potential μ in (6) is determined from the equation for the average number of electrons:

$$n = 1 - \delta = \langle N_i \rangle, \tag{9}$$

where δ is hole doping, $\langle \dots \rangle$ is the statistical average with the Hamiltonian (6).

The HOs satisfy the completeness condition

$$X_i^{00} + X_i^{\sigma\sigma} + X_i^{\bar{\sigma}\bar{\sigma}} = 1\,, \tag{10}$$

which rigorously preserves the constraint of no double occupancy of any quantum state $|i,\alpha\rangle$ on each lattice site i. From the multiplication rules for HOs $X_i^{\alpha\beta}X_i^{\gamma\delta} = \delta_{\beta\gamma}X_i^{\alpha\delta}$ follow the commutation relations:

$$\left[X_i^{\alpha\beta}X_j^{\gamma\delta}\right]_{\pm} = \delta_{ij}\left(\delta_{\beta\gamma}X_i^{\alpha\delta} \pm \delta_{\delta\alpha}X_i^{\gamma\beta}\right), \tag{11}$$

where the upper sign refers to Fermi-type operators such as $X_i^{0\sigma}$, while the lower sign refers to Bose-type operators such as the number (7) or the spin (8) operators.

To study the dynamic charge fluctuations (DCF), we consider the two-time retarded GF [6]

$$\chi_q(t-t') = -\langle\langle N_q(t)|N_q(t')\rangle\rangle = i\theta(t-t')\langle[N_q(t), N_{-q}(t')]\rangle, \tag{12}$$

$$N_{\mathbf{q}} \;=\; \frac{1}{\sqrt{N}}\sum_i N_i \exp(-i\mathbf{q}\,\mathbf{r}_i), \tag{13}$$

where $[A,B] = AB - BA$, $N_q(t) = e^{iHt}N_q e^{-iHt}$ (we take $\hbar = 1$) and $\theta(t-t')$ is the Heaviside function. The DCS $\chi_{\mathbf{q}}(\omega)$ is given by the Fourier transform of the GF (12)

$$\chi_{\mathbf{q}}(\omega) \;=\; -\langle\langle N_{\mathbf{q}}|N_{-\mathbf{q}}\rangle\rangle_\omega = i\int_0^\infty dt e^{i\omega t}\langle[N_{\mathbf{q}}(t), N_{-\mathbf{q}}]\rangle. \tag{14}$$

To calculate GF (12) we consider the density-density relaxation function

$$\Phi_q(t-t') \equiv ((N_q(t)|N_{-q}(t'))) = -i\theta(t-t')(N_q(t), N_{-q}(t')), \tag{15}$$

where

$$(A(t), B) = \int_0^\beta d\lambda < A(t-i\lambda)B >, \tag{16}$$

is Kubo-Mori scalar product, $\beta = \frac{1}{k_B T}$. The Fourier transform of the density-density relaxation function is given by

$$\Phi_{\mathbf{q}}(\omega) = ((N_{\mathbf{q}}|N_{-\mathbf{q}}))_\omega = -i\int_0^\infty dt e^{i\omega t}(N_{\mathbf{q}}(t), N_{-\mathbf{q}}). \tag{17}$$

The DCS $\chi_{\mathbf{q}}(\omega)$ is related to SCS χ_q and the relaxation function $\Phi_q(\omega)$ by the equation

$$\chi_{\mathbf{q}}(\omega) = \chi_{\mathbf{q}} - \omega\Phi_q(\omega). \tag{18}$$

Using the equation of motion method for the time-dependent relaxation function (15), we can write the relaxation function (17) in the form

$$\Phi_{\mathbf{q}}(\omega) \;=\; \chi_{\mathbf{q}}\frac{\omega - \omega M_{\mathbf{q}}(\omega)/m_{\mathbf{q}}}{\omega^2 - \Omega_{\mathbf{q}}^2 - \omega M_{\mathbf{q}}(\omega)/m_{\mathbf{q}}}, \tag{19}$$

where correlation function m_q and the charge excitation energy $\Omega^2_{\mathbf{q}}$ are given by

$$\begin{aligned} m_{\mathbf{q}} &= (i\dot{N}_{\mathbf{q}} \,|\, -i\dot{N}_{-\mathbf{q}}) = \langle\, [i\dot{N}_{\mathbf{q}},\, N_{-\mathbf{q}}]\,\rangle \\ &= \frac{4}{N}\sum_{\mathbf{q}'} [\,t(\mathbf{q}') - t(\mathbf{q}'-\mathbf{q})]\langle X^{\sigma 0}_{\mathbf{q}'} X^{0\sigma}_{\mathbf{q}'}\rangle, \end{aligned} \tag{20}$$

$$\begin{aligned} \Omega^2_{\mathbf{q}} &= \frac{m_q}{\chi_q} = \frac{(-\ddot{N}_{\mathbf{q}}, N_{-\mathbf{q}})}{(N_{\mathbf{q}}, N_{-\mathbf{q}})} = \sum_{\mathbf{q}'} [t(\mathbf{q}') - t(\mathbf{q}-\mathbf{q}')] \\ &\times \left(t(\mathbf{q}') - \frac{1}{2}\,J(\mathbf{q}) + 2V(\mathbf{q}) \right) \langle X^{\sigma 0}_{\mathbf{q}'} X^{0\sigma}_{\mathbf{q}'}\rangle. \end{aligned} \tag{21}$$

The memory function $M_q(\omega)$ is given by the irreducible part of the force-force relaxation function

$$M_{\mathbf{q}}(\omega) = ((F_{\mathbf{q}}|F_{-\mathbf{q}}))^{irr}_{\omega}, \tag{22}$$

where the force $F_{\mathbf{q}} = (d/dt)j_{\mathbf{q}} = \ddot{N}_{\mathbf{q}} = -[[N_{\mathbf{q}}, H], H]$.

Therefore the DCS (14) can be written in the following form

$$\chi_{\mathbf{q}}(\omega) = \chi_{\mathbf{q}} - \omega\Phi_q(\omega) = \frac{m_{\mathbf{q}}}{\Omega^2_{\mathbf{q}} + \omega M_{\mathbf{q}}(\omega)/m_{\mathbf{q}} - \omega^2}. \tag{23}$$

The spectral density of CFs is determined by the relation:

$$I_{\mathbf{q}}(\omega) = \mathrm{Im}\chi_{\mathbf{q}}(\omega + i\varepsilon) = \frac{m_{\mathbf{q}}\, 2\omega\Gamma_{\mathbf{q}}(\omega)}{[\Omega^2_{\mathbf{q}} + 2\omega\Delta_{\mathbf{q}}(\omega) - \omega^2]^2 + [2\omega\Gamma_{\mathbf{q}}(\omega)]^2}, \tag{24}$$

where we introduce the imaginary and real parts of the memory function:

$$\Gamma_{\mathbf{q}}(\omega) = -(1/2\,m_{\mathbf{q}})\mathrm{Im}M_{\mathbf{q}}(\omega + i\varepsilon), \quad \Delta_{\mathbf{q}}(\omega) = (1/2\,m_{\mathbf{q}})\mathrm{Re}M_{\mathbf{q}}(\omega + i\varepsilon). \tag{25}$$

The CF correlation function $\langle N_q N_{-q}\rangle$ in the mean-field approximation (MFA) is given by

$$\langle N_{\mathbf{q}}\, N_{-\mathbf{q}}\rangle = \int_{-\infty}^{\infty} \frac{d\omega}{\exp(\omega/T) - 1}\frac{1}{\pi}\mathrm{Im}\chi(\mathbf{q}, \omega + i\epsilon) = \frac{m_{\mathbf{q}}}{2\Omega_{\mathbf{q}}}\coth\frac{\Omega_{\mathbf{q}}}{2T}. \tag{26}$$

The spectrum of the charge excitations $\Omega^2_{\mathbf{q}}$ along the main directions in the Brillouin zone (BZ) $\Gamma(0,0) \to X(\pi,0) \to M(\pi,\pi) \to \Gamma(0,0)$ is shown in Fig. 3 for hole dopings $\delta = 0.1$ and $\delta = 0.3$ with the standard model parameters $V_1 = 0.3$ and $V_2 = 0.2$ and the temperature $T = 0.02 \sim 90$ K. At the center of the BZ $\Gamma\,(0,0)$ the excitation energy tends to zero, $\Omega^2_{\mathbf{q}} \propto q^2$. At the boundary of the BZ at the point $M\,(\pi,\pi)$ the maximum is observed, and its intensity increases when hole doping decreases. The dispersion of the spectrum depends on the model parameters. It weakly depends on the exchange interaction J but shows a strong variation with the CI parameters V_1 and V_2.

Fig. 4 shows the dependence of $\chi^{-1}_{\mathbf{q}}$ on the parameter V_1 at a fixed $V_2 = 0.2$. As the parameter V_1 increases, the maximum of the SCS (minimum of $\chi^{-1}_{\mathbf{q}}$) shifts from the point $X\,(\pi,0)$ to the point $M\,(\pi,\pi)$. At $V_1 \gtrsim 0.5$ the inverse charge susceptibility becomes negative near this point, which

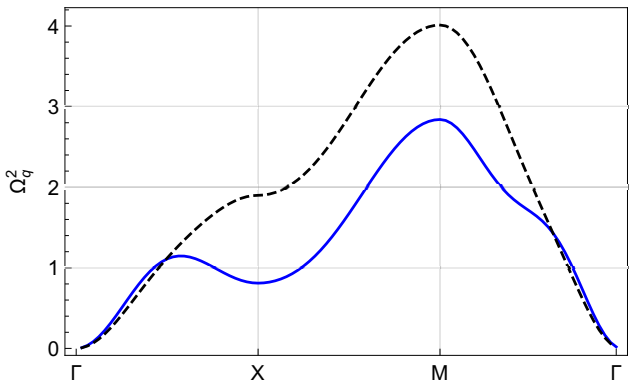

Fig. 3: Spectrum of charge excitations Ω_q^2 along the main directions in the BZ: $\Gamma(0,0) \to X(\pi,0) \to M(\pi,\pi) \to \Gamma(0,0)$ for $\delta = 0.3$ (blue, solid line), $\delta = 0.1$ (black, dashed line).

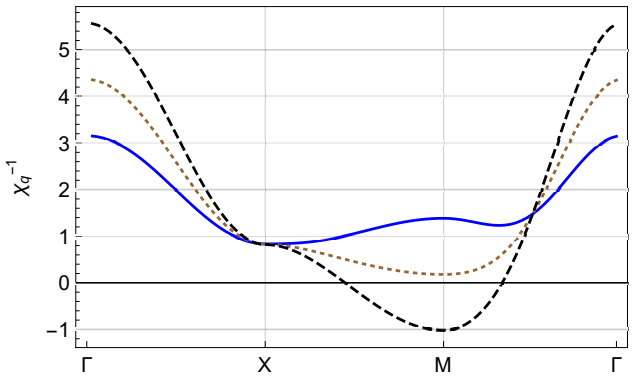

Fig. 4: Inverse SCS χ_q^{-1} for $\delta = 0.3$ at $V_2 = 0.2$ depending on the parameter V_1: $V_1 = 0.3$ (blue, solid line), $V_1 = 0.6$ (brown, dotted line), $V_1 = 0.9$ (black, dashed line).

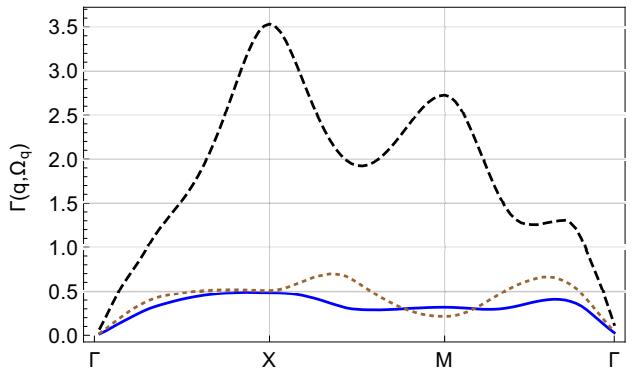

Fig. 5: $\Gamma(q,\Omega_q)$ at temperature $T = 0.02$ for $\delta = 0.3$ (blue, solid line), $\delta = 0.2$ (brown, dotted line), $\delta = 0.1$ (black, dashed line).

indicates instability of the uniform charge distribution and formation of the CDW. Therefore, depending on the CI parameters V_1 and V_2, which have different symmetries, CDWs can arise either along the direction $\Gamma(0,0) \to M(\pi,\pi)$ as V_1 increases, or along $\Gamma(0,0) \to X(\pi,0)$ as V_2 increase.

Fig. 5 demonstrate the damping at the charge excitation energy $\Gamma(\mathbf{q}, \omega = \Omega_{\mathbf{q}})$. The largest damping occurs at $X(\pi,0)$ and $M(\pi,\pi)$ points of the BZ. The damping is greatly increased at low hole doping as shown for $\delta = 0.1$ where electron correlations are strong. In that case the damping $\Gamma(\mathbf{q},\omega)$ becomes of the order of the charge excitation energy $\Omega_{\mathbf{q}}$ that results in a broad spectrum of the spectral density $I(\mathbf{q},\omega)$. For larger hole doping, in particular at $\delta = 0.3$, the damping is much weaker, $\Gamma(\mathbf{q},\omega) \sim 0.5$, and a sharp peak in $I(\mathbf{q},\omega)$ emerges at high energy of the order of the charge excitation energy $\Omega_{\mathbf{q}} = 1 - 1.5$. Similar maximum in CFs was found in the QMC simulation for the Hubbard model in Ref [7] [see Fig. 4.2(b)].

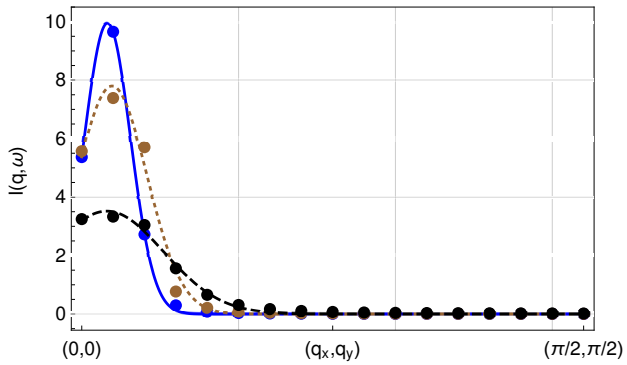

Fig. 6: Spectral density $I((q_x, q_y = q_x), \omega = 0.05)$ along the direction $\Gamma(0,0) \to M(\pi,\pi)$ at temperature $T = 0.02$ for $\delta = 0.3$ (blue, solid line), $\delta = 0.2$ (brown, dotted line), $\delta = 0.1$ (black, dashed line).

The dispersions of low-energy charge excitation for $\omega = 0.05 \approx 20$ meV are shown in Fig. 6 along the directions $\Gamma(0,0) \to M(\pi,\pi)$. We observe a maximum in excitations at small wave-vectors which are found at low doping and sharper and more intensive at smaller doping. The intensity of excitations along $\Gamma(0,0) \to X(\pi,0)$ is higher in comparison with the diagonal direction $\Gamma(0,0) \to M(\pi,\pi)$ due to weaker CI in the latter case $V_2 < V_1$. In experiments for various cuprates, the charge density mudulation is observed, along the $Cu-O$ bonds which is explained by a stronger coupling along the bonds. The main results of this chapter are published in Refs.2,3 from the List of publications above.

In the **Third Chapter** we consider electronic spectrum and superconducting pairing in the extended $t-J-V$ model on a square lattice. To study strong electron correlations in the singly occupied subband of the t–J model one has to use the projected electron operators, as $\widetilde{a}^{\dagger}_{i\sigma} = a^{\dagger}_{i\sigma}(1-$

$N_{i\bar{\sigma}}$). Here $a^{\dagger}_{i\sigma}$ is a creation electron operator on the lattice site i with spin $\sigma/2$, $\sigma = \pm 1$ ($\bar{\sigma} = -\sigma$) and $N_{i\bar{\sigma}} = \widetilde{a}^{\dagger}_{i\bar{\sigma}}\widetilde{a}_{i\bar{\sigma}}$ is the number operator. The t–J model in the conventional notation reads [8]:

$$H = -\sum_{i\neq j,\sigma} t_{ij}\widetilde{a}^{+}_{i\sigma}\widetilde{a}_{j\sigma} + \frac{1}{2}\sum_{i\neq j} J_{ij}\left(\mathbf{S}_i\mathbf{S}_j - \frac{1}{4}N_iN_j\right) + H_{c,ep}, \tag{27}$$

where $S^{\alpha}_i = (1/2)\sum_{s,s'}\widetilde{a}^{+}_{is}\sigma^{\alpha}_{s,s'}\widetilde{a}_{is'}$ are spin-1/2 operators, $\sigma^{\alpha}_{s,s'}$ is the Pauli matrix. Here t_{ij} is the hopping parameter between i and j lattice sites and J_{ij} is the AFM exchange interaction. The intersite CI V_{ij} for electrons and EPI g_{ij} are taken into account by the Hamiltonian:

$$H_{c,ep} = \frac{1}{2}\sum_{i\neq j} V_{ij}N_iN_j + \sum_{i,j} g_{ij}N_i\,u_j, \tag{28}$$

where u_j describe atomic displacements on the lattice site j for phonon modes.

The unconventional commutation relations for the projected electron operators result in the kinematical interaction. For instance, if we consider commutation relation for the projected electron creation $\widetilde{a}^{\dagger}_{j\sigma}$ and annihilation $\widetilde{a}_{i\sigma}$ operators,

$$\widetilde{a}_{i\sigma}\widetilde{a}^{\dagger}_{j\sigma} + \widetilde{a}^{\dagger}_{j\sigma}\widetilde{a}_{i\sigma} = \delta_{ij}(1 - N_{i\sigma}/2 + \sigma S^{z}_i), \tag{29}$$

we observe that they are Fermi operators on different lattice sites but on the same lattice site they describe the **kinematical interaction** of electrons with charge $N_{i\sigma}$ and spin S^{α}_i fluctuations. This kinematical interaction was considered in calculation of the self-energy at first in Ref. [9] and later in Ref. [10].

It is convenient to describe the projected electron operators by the HOs, as, e.g., $\widetilde{a}^{+}_{i\sigma} = X^{\sigma 0}_i$. Using the HOs, we write the Hamiltonian (27) in the form

$$\begin{aligned} H &= -\sum_{i\neq j,\sigma} t_{ij}X^{\sigma 0}_i X^{0\sigma}_j - \mu\sum_{i\sigma} X^{\sigma\sigma}_i \\ &+ \frac{1}{4}\sum_{i\neq j,\sigma} J_{ij}\left(X^{\sigma\bar{\sigma}}_i X^{\bar{\sigma}\sigma}_j - X^{\sigma\sigma}_i X^{\bar{\sigma}\bar{\sigma}}_j\right) + H_{c,ep}, \end{aligned} \tag{30}$$

where we introduced the chemical potential μ. To discuss the electronic spectrum and superconducting pairing within the model we consider the retarded two-time GF [6]:

$$\begin{aligned} \widehat{G}_{ij,\sigma}(t-t') &= -i\theta(t-t')\langle\{\Psi_{i\sigma}(t), \Psi^{+}_{j\sigma}(t')\}\rangle \\ &\equiv \langle\langle \Psi_{i\sigma}(t) \,|\, \Psi^{+}_{j\sigma}(t')\rangle\rangle, \end{aligned} \tag{31}$$

where $\{A, B\} = AB + BA$ and we introduced HOs in the Nambu notation:

$$\Psi_{i\sigma} = \begin{pmatrix} X^{0\sigma}_i \\ X^{\bar{\sigma}0}_i \end{pmatrix}, \qquad \Psi^{+}_{i\sigma} = \left(X^{\sigma 0}_i \; X^{0\bar{\sigma}}_i\right). \tag{32}$$

Introducing the Fourier representation in $(\mathbf{k}, \omega)$-space for the GF (31)

$$\widehat{G}_{ij\sigma}(t-t') = \frac{1}{2\pi}\int_{-\infty}^{\infty} dt e^{-i\omega(t-t')}\widehat{G}_{ij\sigma}(\omega), \tag{33}$$

$$\widehat{G}_{ij\sigma}(\omega) = \frac{1}{N}\sum_{\mathbf{k}} \exp[\mathbf{k}(\mathbf{r_i} - \mathbf{r_j})]\,\widehat{G}_{\sigma}(\mathbf{k}, \omega), \tag{34}$$

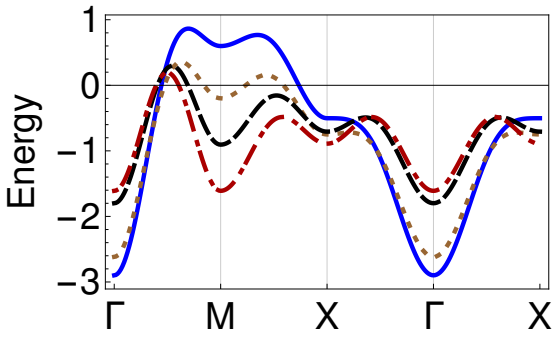

Fig. 7: Dispersion of the electron spectrum for $\delta = 0.05$ (red, dash-dotted line), $\delta = 0.1$ (black, dashed line), $\delta = 0.2$ (brown, dotted line), $\delta = 0.3$ (blue, solid line).

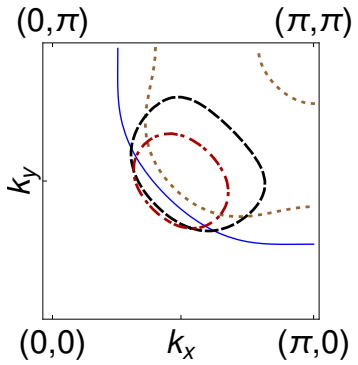

Fig. 8: Fermi surface (FS) in the quarter of the BZ for $\delta = 0.05$ (red, dash-dotted line), $\delta = 0.1$ (black, dashed line), $\delta = 0.2$ (brown, dotted line), $\delta = 0.3$ (blue, solid line).

we represent it as the matrix

$$\widehat{G}_\sigma(\mathbf{k},\omega) = \begin{pmatrix} G_\sigma(\mathbf{k},\omega) & F_\sigma(\mathbf{k},\omega) \\ F^\dagger_\sigma(\mathbf{k},\omega) & -G_{\bar\sigma}(-\mathbf{k},-\omega) \end{pmatrix}, \tag{35}$$

where $G_\sigma(\mathbf{k},\omega)$ and $F_\sigma(\mathbf{k},\omega)$ are the normal and anomalous parts of the GF (31).

By differentiating the GF (31) over the times t and t' we can obtain the Dyson equation in the exact form

$$\widehat{G}_{ij\sigma}(\omega) = \widehat{G}^0_{ij\sigma}(\omega) + \sum_{kl} \widehat{G}^0_{ik\sigma}(\omega)\; Q^{-1}\, \widehat{\Sigma}_{kl\sigma}(\omega)\; \widehat{G}_{lj\sigma}(\omega), \tag{36}$$

where $Q = 1 - n/2$. Here the zero–order GF in generalized MFA (GMFA) has the form:

$$\widehat{G}^0_\sigma(\mathbf{k},\omega) = Q\frac{\omega\hat\tau_0 + \varepsilon(\mathbf{k})\hat\tau_3 + \Delta_\sigma(\mathbf{k})\hat\tau_1}{\omega^2 - E^2(\mathbf{k})}, \tag{37}$$

where $\hat\tau_0,\ \hat\tau_1,\ \hat\tau_3$ are the Pauli matrices and $E^2(\mathbf{k}) = \varepsilon^2(\mathbf{k}) + \Delta^2_\sigma(\mathbf{k})$ is the energy of quasiparticle (QP) excitations in the superconducting state. The self–energy operator $\widehat{\Sigma}_{kl\sigma}(\omega)$ is given by the *proper* part of the scattering matrix that has no parts connected by the single zero-order GF:

$$\widehat{\Sigma}_{ij\sigma}(\omega) = \langle\langle \widehat{Z}^{(irr)}_{i\sigma} \mid \widehat{Z}^{(irr)^+}_{j\sigma} \rangle\rangle^{\rm proper}_\omega Q^{-1} = \begin{pmatrix} M_{ij\sigma}(\omega) & \Phi_{ij\sigma}(\omega) \\ \Phi^\dagger_{ij\sigma}(\omega) & -M_{ij\bar\sigma}(\omega) \end{pmatrix}. \tag{38}$$

The functions $M_{ij\sigma}(\omega)$ and $\Phi_{ij\sigma}(\omega)$ denote the respective normal and anomalous (pair) components of the self-energy operator. Therefore, for the single–electron GF (35) we obtain an exact representation:

$$\widehat{G}_\sigma(\mathbf{k},\omega) = Q\{\omega\hat\tau_0 - \widehat{E}_\sigma(\mathbf{k}) - \widehat{\Sigma}_\sigma(\mathbf{k},\omega)\}^{-1}. \tag{39}$$

The normal state GF in the GMFA is given by the GF (39)

$$G^0(\mathbf{k},\omega) = \langle\langle X^{0\sigma}_{\mathbf{k}} | X^{\sigma 0}_{\mathbf{k}} \rangle\rangle_\omega = \frac{Q}{\omega - \varepsilon(\mathbf{k})}. \tag{40}$$

Here the electronic energy is determined by the relation:

$$\varepsilon(\mathbf{k}) = -4t\,\alpha\gamma(\mathbf{k}) - 4t'\,\beta\gamma'(\mathbf{k}) - 4t''\,\beta\gamma''(\mathbf{k}) + \omega^{(c)}(\mathbf{k}) - \mu, \tag{41}$$

$$\omega^{(c)}(\mathbf{k}) = \frac{1}{N}\sum_{\mathbf{q}} V(\mathbf{k}-\mathbf{q})N(\mathbf{q}), \tag{42}$$

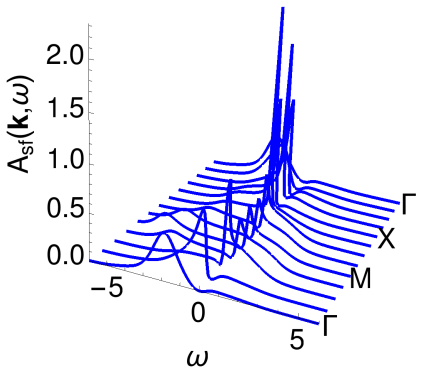

Fig. 9: Spectral density $A(\mathbf{k},\omega)$ for $\delta = 0.1$.

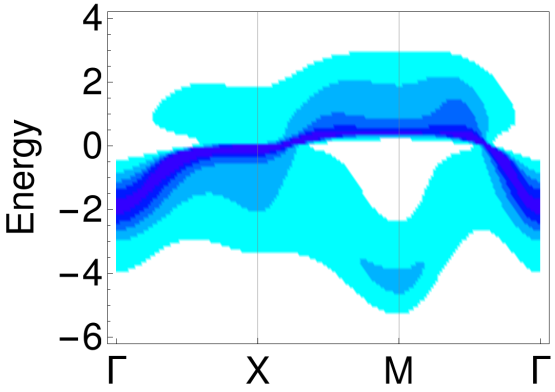

Fig. 10: Energy dispersion for $\delta = 0.1$.

where $\gamma(\mathbf{k}) = (1/2)(\cos k_x + \cos k_y)$, $\gamma'(\mathbf{k}) = \cos k_x \cos k_y$, $\gamma''(\mathbf{k}) = (1/2)(\cos 2k_x + \cos 2k_y)$ and the hopping parameters are given by $t' = 0.1t$, $t'' = 0.2t$. We take $t = 0.4$ eV as the energy unit.

The hopping parameters are renormalized by the short-range AFM correlations given by the parameters:

$$\alpha = Q\left(1 + C_1/Q^2\right),\ \beta = Q\left(1 + C_2/Q^2\right), \tag{43}$$

which depend on the spin correlation functions for the first and the next neighbors:

$$\begin{aligned} C_1 &= \langle \mathbf{S}_i \mathbf{S}_{i\pm a_x/a_y} \rangle = \frac{1}{N}\sum_{\mathbf{q}} \gamma(\mathbf{q})\, C_{\mathbf{q}}, \\ C_2 &= \langle \mathbf{S}_i \mathbf{S}_{i\pm a_x \pm a_y} \rangle = \frac{1}{N}\sum_{q} \gamma'(\mathbf{q})\, C_{\mathbf{q}}. \end{aligned} \tag{44}$$

For the spin correlation function $C_{\mathbf{q}} = \langle \mathbf{S}_{\mathbf{q}} \mathbf{S}_{-\mathbf{q}} \rangle$ we take the model:

$$C_{\mathbf{q}} = \frac{C_{\mathbf{Q}}}{1 + \xi^2[1 + \gamma(\mathbf{q})]}, \tag{45}$$

where the parameter $C_{\mathbf{Q}}$ is defined from the normalization condition $\langle \mathbf{S_i S_i} \rangle = (3/4)n = (1/N)\sum_{\mathbf{q}} C_{\mathbf{q}}$.

This renormalization of the spectrum results in the well defined electronic spectrum shown in Fig.7 which changes with hole doping since the AFM correlation functions (44) strongly depends on the electron concentration. The corresponding FS $\varepsilon(\mathbf{k}_{\mathrm{F}}) = 0$ is also transforms with doping from the four hole pockets form at low doping to the large FS as shown in Fig.8. By taking into account the self-energy contribution in the GF (39) instead of the well defined in the GMFA electronic spectrum in Fig.7 we observe a diffuse spectral density. At the same time, the FS in Fig.8 in the form of closed pockets for low doping transforms to open arcs representing the parts of the FS close to $(\pi/2, \pi/2)$ point of the BZ which do not shift considerably with doping. This transformation is observed in angle-resolved photoemission spectroscopy (ARPES) experiments [11–13].

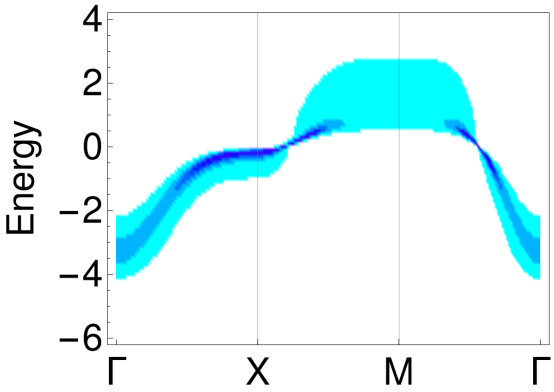

Fig. 11: Energy dispersion for $\delta = 0.3$.

The self-energy (38) is determined by the many-particle GFs where the normal and anomalous (pairs) components are given by:

$$M_{ij\sigma}(\omega) = (1/Q)\,\langle\langle [X_i^{0\sigma}, H]|[H, X_j^{\sigma 0}]\rangle\rangle_\omega, \tag{46}$$

$$\Phi_{ij\sigma}(\omega) = (1/Q)\,\langle\langle [X_i^{0\sigma}, H]|[X_j^{0\bar{\sigma}}, H]\rangle\rangle_\omega. \tag{47}$$

Using the the spectral representation we represent them in terms of the time-dependent correlation functions which are calculated in the SCBA where propagation of Fermionic and Bosonic excitation on different lattice sites is assumed to be independent:

$$\langle X_m^{\sigma' 0} B^+_{j\sigma\sigma'}|X_l^{0\sigma'}(t)B_{i\sigma\sigma'}(t)\rangle = \langle X_m^{\sigma' 0} X_l^{0\sigma'}(t)\rangle\langle B^+_{j\sigma\sigma'} B_{i\sigma\sigma'}(t)\rangle\ , \tag{48}$$

$$\langle X_m^{\bar{\sigma}' 0} B_{j\bar{\sigma}\bar{\sigma}'}|X_l^{\sigma' 0}(t)B_{i\sigma\sigma'}(t)\rangle = \langle X_m^{\bar{\sigma}' 0} X_l^{\sigma' 0}(t)\rangle\,\langle B_{j\bar{\sigma}\bar{\sigma}'} B_{i\sigma\sigma'}(t)\rangle\,. \tag{49}$$

Calculation of the corresponding single-particle correlation functions in these equations results in the self-energy

$$M(\mathbf{k},\omega) = \frac{1}{N}\sum_{\mathbf{q}}\int_{-\infty}^{+\infty}\frac{dz}{\pi Q}\,K^{(+)}(\omega,z,\mathbf{k},\mathbf{q})[-\mathrm{Im}]\,\mathrm{G}(\mathbf{q},\mathrm{z}), \tag{50}$$

$$\Phi_\sigma(\mathbf{k},\omega) = \frac{1}{N}\sum_{\mathbf{q}}\int_{-\infty}^{+\infty}\frac{dz}{\pi Q}\,K^{(-)}(\omega,z,\mathbf{k},\mathbf{q})[-\mathrm{Im}]\mathrm{F}_\sigma(\mathbf{q},\mathrm{z}). \tag{51}$$

The kernel of the integral equations is defined as

$$K^{(\pm)}(\omega,z,\mathbf{k},\mathbf{q}) = \int_{-\infty}^{+\infty}\frac{\mathrm{d}\Omega}{2\pi}\,\frac{\tanh(z/2T)+\coth(\Omega/2T)}{\omega-z-\Omega}$$
$$\times\Big\{|t(\mathbf{q})|^2\mathrm{Im}\chi_{sf}(\mathbf{k}-\mathbf{q},\Omega)\pm|g_{ep}(\mathbf{k}-\mathbf{q})|^2\mathrm{Im}\chi_{ph}(\mathbf{k}-\mathbf{q},\Omega)$$
$$\pm\left[|V(\mathbf{k}-\mathbf{q})|^2+|t(\mathbf{q})|^2/4\right]\mathrm{Im}\,\chi_{cf}(\mathbf{k}-\mathbf{q},\Omega)\Big\}$$
$$\equiv\int_{-\infty}^{+\infty}\frac{\mathrm{d}\Omega}{2\pi}\,\frac{\tanh(z/2T)+\coth(\Omega/2T)}{\omega-z-\Omega}\lambda^{(\pm)}(\mathbf{k},\mathbf{q},\Omega). \tag{52}$$

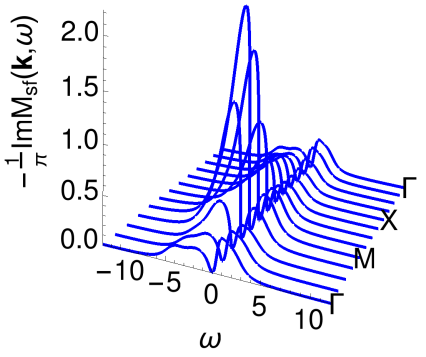

Fig. 12: Imaginary part of the spin-fluctuation self-energy $-(1/\pi)\mathrm{Im}M_{sf}(\mathbf{k},\omega)$ for $\delta = 0.1$.

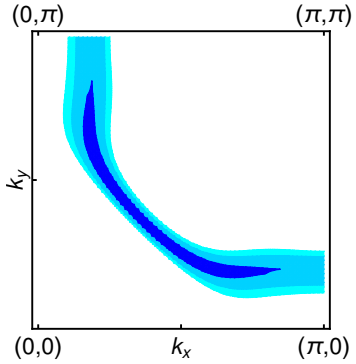

Fig. 13: Spectral density $A(\mathbf{k},0)$ in the quarter of the BZ for $\delta = 0.05$.

The spectral densities of bosonic excitations are determined by the dynamic susceptibility for spin (sf), number (charge) (cf), and lattice (phonon) (ph) fluctuations

$$\chi_{sf}(\mathbf{q},\omega) = -\langle\langle \mathbf{S}_{\mathbf{q}} | \mathbf{S}_{-\mathbf{q}} \rangle\rangle_{\omega}, \tag{53}$$

$$\chi_{cf}(\mathbf{q},\omega) = -\langle\langle \delta N_{\mathbf{q}} | \delta N_{-\mathbf{q}} \rangle\rangle_{\omega}, \tag{54}$$

$$\chi_{ph}(\mathbf{q},\omega) = -\langle\langle u_{\mathbf{q}} | u_{-\mathbf{q}} \rangle\rangle_{\omega}. \tag{55}$$

Let us consider the electronic spectrum in the normal state which is determined by normal state GF in Eq. (39)

$$G(\mathbf{k},\omega) = \langle\langle X^{0\sigma}_{\mathbf{k}} | X^{\sigma 0}_{\mathbf{k}} \rangle\rangle = \frac{Q}{\omega - \varepsilon(\mathbf{k}) - M(\mathbf{k},\omega)}. \tag{56}$$

The normal state self-energy is given by Eqs. (50), (52). The spectral density of electronic excitations is determined by

$$A(\mathbf{k},\omega) = -\frac{1}{\pi Q}\mathrm{Im}G(\mathbf{k},\omega + i\epsilon) = \frac{-M''(\mathbf{k},\omega)/\pi}{[\omega - \varepsilon(\mathbf{k}) - M'(\mathbf{k},\omega)]^2 + [M''(\mathbf{k},\omega)]^2}. \tag{57}$$

Here we introduce the real, $M'(\mathbf{k},\omega)$, and imaginary, $M''(\mathbf{k},\omega)$, parts of the self-energy: $M(\mathbf{k},\omega + i\epsilon) = M'(\mathbf{k},\omega) + iM''(\mathbf{k},\omega)$. The renormalization parameter for the electronic energy close to the FS, $\omega \to 0$, reads:

$$Z_{\mathbf{k}}(0) = 1 - [\partial M'(\mathbf{k},\omega)/\partial\omega]_{\omega=0} \equiv 1 + \lambda(\mathbf{k}), \tag{58}$$

where $\lambda(\mathbf{k})$ is the coupling parameter.

The self-energy and the spectral density are calculated by iteration. The results of the 10-th order of iterations for the spectral density for the electron interaction with spin-fluctuations $A_{sf}(\mathbf{k},\omega)$ (57) and the energy dispersion $\tilde{\varepsilon}(\mathbf{k})$ along the main directions in the BZ, $\Gamma\,(0,0) \to X\,(\pi,0) \to M\,(\pi,\pi) \to \Gamma\,(0,0)$, are presented in Figs. 9 – 11.

At low doping the spectral density shows a large incoherent background, in particular close to the (π,π)-point of the BZ, as shown in Figs. 9, 10 for $\delta = 0.1$. With increasing doping the

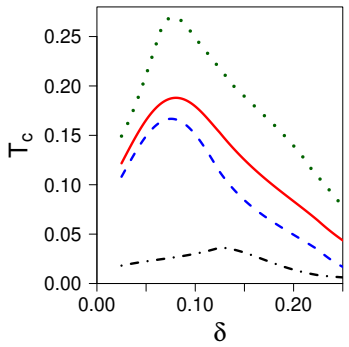

Fig. 14: (Color online) Solution of the gap equation (59) in the WCA, $Z = 1$, for T_c^{ep} (black, dash-dotted ed line), T_c^{sf} (blue, dashed line), and T_c^{sf+ep} (red, solid line). The green dotted line show T_c^{sf+ep} with zero CI, $V(\mathbf{k}-\mathbf{q}) = 0$.

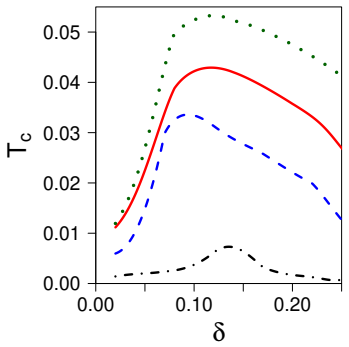

Fig. 15: (Color online) Solution of the gap equation (59) in the SCA for T_c^{ep} (black, dash-dotted line), T_c^{sf} (blue, dashed line), and T_c^{sf+ep} (red, solid line). The green dotted line show T_c^{sf+ep} with zero CI, $V(\mathbf{k}-\mathbf{q}) = 0$.

spin-fluctuation interaction becomes weak and the incoherent background decreases, as shown in Fig. 11 for $\delta = 0.3$. The spectrum of excitations in Fig. 11 is close to that one in the GMFA shown in Fig. 7. However, at low doping where the self-energy renormalization is strong the spectrum in the GMFA is quite different from those shown in Fig 10. In particular, a large intensity of excitations at the (π, π)-point of the BZ appears at much lower energy than in the GMFA due to a shift of the excitation energy caused by the real part of the self-energy. Therefore, we can conclude that the self-energy effects are very important in studies of the QP excitations in the t-J model.

The QP damping determined by the imaginary part of the self-energy (50) $\Gamma(\mathbf{k}, \omega) = -(1/\pi)\mathrm{Im}M_{sf}(\mathbf{k}, \omega)$ due to spin-fluctuation interaction is plotted in Fig. 12 at doping $\delta = 0.1$. For a larger doping, $\delta = 0.3$, the intensity of the QP damping decreases and the large FS emerges as in the GMFA.

The results of spectral density close to the FS $A_{sf}(\mathbf{k}, \omega = 0)$ (57) which determines the FS are presented in Figs. 13 for low doping. It reveals the arc-type form which transforms to the large FS for high doping as in the GMFA. This FS transformation from the arc-type at low doping to the large FS at high doping is observed in ARPES experiments (see, e.g., Refs. [11–14]. Similar results were obtained using the cluster perturbation theory (CPT) for the t-J model in Ref. [15] and for the Hubbard model in Ref. [16].

Let us consider the superconducting state. The gap equation close to the FS, $\phi_\sigma(\mathbf{k}) = \phi_\sigma(\mathbf{k}, \omega = 0)$, is given by the equation:

$$\phi_\sigma(\mathbf{k}) = \frac{1}{N}\sum_{\mathbf{q}}\int_{-\infty}^{+\infty}\frac{dz}{\pi}\left[\frac{V(\mathbf{k}-\mathbf{q}) - J(\mathbf{k}-\mathbf{q})}{\exp(z/T)+1} + K^{(-)}(0, z, \mathbf{k}, \mathbf{q})\right] \times[-\mathrm{Im}]\frac{\phi_\sigma(\mathbf{q})}{\mathrm{Z}_{\mathbf{q}}^2(0)\left[(\mathrm{z}+\mathrm{i}\epsilon)^2 - \widetilde{\varepsilon}^2(\mathbf{q}, \mathrm{z})\right]}. \quad (59)$$

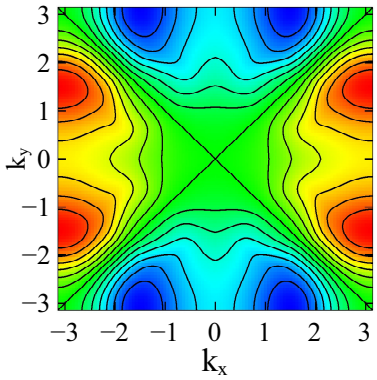

Fig. 16: (Color online) Wave-vector dependence of the superconducting gap at the FS $\phi(\mathbf{q})$.

The first contribution in this equation given by the AFM exchange interaction $J(\mathbf{k}-\mathbf{q})$ is due to the GMFA and gives quite high $T_c \sim 100$ K as proposed by Anderson [8] and considered later in many publications. However, if we take into account the intersite CI $V(\mathbf{k}-\mathbf{q})$ which is of the same order in cuprates as $J(\mathbf{k}-\mathbf{q})$, we obtain very low $T_c \sim 10^{-3}$ K . Therefore, the Anderson theory cannot explain high-T_c in cuprates. Only consideration of spin fluctuation contribution can results in high-T_c as discussed below.

Solution of the gap equation (59) in the weak-coupling approximation (WCA), $Z(\mathbf{q}) = 1$, for T_c as a function of doping is presented in Fig. 14. Solution of the gap equation (59) for T_c in the strong-coupling approximation (SCA) for $Z(\mathbf{q})$ is shown in Fig. 15. To simplify the numerical calculation we approximated the function $Z(\mathbf{q})$ by its average over $\mathbf{q}$ values: $Z = 2.5 - 4\delta$. The superconducting T_c in the SCA in Fig. 15 is an order of magnitude smaller than in the WCA in Fig. 14 due to suppression of the QP weight given by $1/Z(\mathbf{q})$. We note that the effect of CI, shown by the green dotted line, only weakly decreases the T_c both in the WCA and SCA.

Comparison of T_c in the WCA in Fig. 14 and in the SCA in Fig. 15 shows that in both approximations the contribution from the EPI is noticeably smaller than those induced by the spin-fluctuation interaction. We can explain this as follow: While in summation over $\mathbf{q}$ contributions to the normal self-energy come from all symmetry components of interactions, in the gap equation contributions are restricted only to the B_{1g} symmetry component of interactions determined by the symmetry of the d-wave gap $\phi_\sigma(\mathbf{q})$. In particular, a strong momentum-independent EPI gives no contribution to the gap equation but results in a large contribution to the normal self-energy and the parameter $Z(\mathbf{q})$ in the gap equation that suppresses T_c (see also Ref. [17]). Therefore, the EPI can be quite strong and gives observable polaronic effects but has a small d-wave partial harmonic and plays only a secondary role in the d-wave pairing. This results in the weak isotope effect on T_c in the optimally doped cuprates. The same holds for the intersite CI since only d-wave partial harmonic gives a contribution to the gap equation as shown in Figs. 14 and 15. This explains why the strong single-site CI cannot destroy the superconductivity (see Refs. [5, 18]).

The wave-vector dependence of the superconducting gap at the FS $\phi(\mathbf{q})$ at $\delta = 0.2$ is presented in Fig. 16 in the BZ. We see that the maximum values of the gap are shifted in comparison

with the model d-wave gap function $\phi^{(0)}(\mathbf{q}) = \phi^{(0)}(\cos k_x - \cos k_y)$ from the BZ boundary at $(0, \pm\pi), (\pm\pi, 0)$ points. Similar behavior was found in Ref. [19] in the t–J^* model with hopping parameters between distant lattice sites. The main results of this chapter are published in Ref.4 from the List of publications above.

Conclusion The main results of the dissertation are given below:

1. We have studied the metal-insulator transition in the half-filled ionic Hubbard model using CPA. For a fixed and finite Δ two transitions from BI via metal to MI are found by changing value of Coulomb repulsion U. The calculation of temperature dependent conductivity demonstrated that for intermediate and large Δ the largest conductivity occurs near the special value $U = 2\Delta$ at all temperature. For a fixed Δ the region of finite conductivity $[U_{c1}, U_{c2}]$ expands and its maximum decreases with increasing T. Our results are in good agreement with the ones obtained by the DQMC simulation. The calculation presented here can be extended to the optical conductivity.

2. We have considered behavior of the static $\chi_{\mathbf{q}}$ and dynamics $\chi_q(\omega)$ charge susceptibility in a system of electrons with strong correlations in the framework of the t-J-V model. We have shown that for a sufficiently strong intersite Coulomb repulsion, $\chi_{\mathbf{q}}$ increases without limit ($\chi_{\mathbf{q}}^{-1}$ vanishes), and CDWs arise in the system either along the diagonal of the unit cell (near the point $M\,(\pi, \pi)$ of the BZ) or along the edge of the unit cell (near the point $X\,(\pi, 0)$ of the BZ). The dependence on other model parameters including the AFM exchange interaction J, is weaker. Taking into account the damping of CFs described by the imaginary part of the memory function we have found out that at low hole doping, e.g., for $\delta = 0.1$ due to strong correlations only a broad spectrum of overdamped CFs is observed. At large hole doping, the Fermi-like type behavior emerges and well-defined high-energy charge excitations appear close to $M(\pi, \pi)$ and $X(\pi, 0)$ points of the BZ. The dispersion of low-energy excitations demonstrates a maximum at small wave vectors with the higher intensity in comparison with experiments at high doping but with a weaker intensity at small doping in comparison with experiments.

3. A detailed study of the electronic spectrum and superconductivity for strongly correlated electronic systems within the microscopic theory for the extend $t - J$ model is presented. Besides the conventional AFM exchange interaction J, the EPI and the intersite Coulomb repulsion are taken into account. The projection technique was employed to obtain the exact Dyson equation for the normal and anomalous (pairs) GF's in terms of Hubbard operators. The self-energy given by many-particle GF's was calculated in the SCBA in the second order of interaction. The most important contribution is induced by the kinematical interaction for the HOs. It results in strong coupling of electrons with spin fluctuations of the order of hopping parameter $t(\mathbf{q})$ much larger than the exchange interaction $J(\mathbf{q})$. Therefore, we suggest that the spin-fluctuation pairing is the mechanism high-T_c in cuprates.

Acknowledgements

I would like to thank my first supervisor prof. Nikolai Maksimilianovich Plakida for providing guidance throughout this work and the willingness to impart his knowledge for many years I spent in Dubna. His passing from life was a huge loss for all of us.

I thank my second supervisor, prof. V. Yu. Yushankhai for his support and encouragement at the final stage of preparing the dissertation for defense. His thoughtful comments and recommendations were very valuable for me.

I would like to thank my co-author A.A. Vladimirov for help with numerical calculations as well as V.S. Oudovenko who took the time to answer my numerous questions in detail.

I express my gratitude to the leadership of the Laboratory of Theoretical Physics, namely, personally to profs. D. I. Kazakov and V.A. Osipov for creating favorable conditions that allow me to complete the dissertation.

The author also thanks profs. Le Hong Khiem and Hoang Anh Tuan for helpful advice and financial support during the author's time at Dubna.

References

[1] N. Paris et al., Phys. Rev. Lett. **98** (2007) 046403.

[2] K. Bouadim et al., Phys. Rev. B **76** (2007) 085112.

[3] J. Hubbard, "Electron correlations in narrow energy bands. IV. The atomic representation", Proc. Roy.Soc. A (London) **285** (1965) 542.

[4] Yu.A. Izyumov and Yu. N. Scryabin, Statistical Mechanics of Magnetically Ordered Systems, New York: Consultant Bureau, 1989.

[5] N. M. Plakida and V. S. Oudovenko, "On the theory of superconductivity in the extended Hubbard model: Spin-fluctuation pairing", Eur. Phys. J. B **86** (2013) 115 (1–15).

[6] D.N. Zubarev, Usp. Fiz. Nauk **71** (1960) 71; (Sov. Phys. Usp. **3** (1960) 320).

[7] N. Bulut, Adv. Phys. 51 (2002) 1587.

[8] P. W. Anderson, Science **235** (1987) 1196; P. W. Anderson, The theory of superconductivity in the high-T_c cuprates, Princeton University Press, Princeton, 1997.

[9] N. M. Plakida, V. S. Oudovenko, "Electron spectrum and superconductivity in the t–J model at moderate doping", Phys. Rev. B **59** (1999) 11949–11961.

[10] P. Prelovšek and A. Ramšak, Phys. Rev. B **72** (2005) 012510.

[11] A. A. Kordyuk, S. V. Borisenko, M. S. Golden, S. Legner, K. A. Nenkov, M. Knupfer, J. Fink, H. Berger, L. Forro, and R. Follath, Phys. Rev. B **66** (2002) 014502.

[12] K. M. Shen, F. Ronning, D. H. Lu, F. Baumberger, N. J. C. Ingle, W. S. Lee, W. Meevasana, Y. Kohsaka, M. Azuma, M. Takano, H. Takagi, and Z.-X. Shen, Science **307** (2005) 901.

[13] M. Hashimoto, T. Yoshida, H. Yagi, M. Takizawa, A. Fujimori, M. Kubota, K. Ono, K. Tanaka, D.H. Lu, Z.-X. Shen, S. Ono, and Yoichi Ando, Phys. Rev. B **77** (2008) 094516.

[14] W.S. Lee, I.M. Vishik, K. Tanaka, D.H. Lu, T. Sasagawa, N. Nagaosa, T.P. Devereaux, Z. Hussainand, and Z.-X. Shen, Nature **450** (2007) 81.

[15] M. Kohno, Phys. Rev. B **92** (2015) 085128.

[16] V. I. Kuz'min, M. A. Visotin, S. V. Nikolaev, and S. G. Ovchinnikov, Phys. Rev. B **101** (2020) 115141.

[17] A.I. Lichtenstein and M.L. Kulić, Physica C **245** (1995) 186.

[18] E. Plekhanov, S. Sorella, and M. Fabrizio, Phys. Rev. Lett. **90** (2003) 187004.

[19] V. V. Val'kov and D. M. Dzebisashvili, JETP Lett. **77** (2003) 381.